

Peat subsidence and dynamics in Midden-Delfland, the Netherlands, from time series InSAR analysis and the SPAMS model

Lumban-Gaol, Yustisi; Conroy, Philip; van Diepen, Simon; van Leijen, Freek; Hanssen, Ramon

10.1016/j.geoderma.2025.117551

Publication date

Document Version Final published version

Published in Geoderma

Citation (APA)
Lumban-Gaol, Y., Conroy, P., van Diepen, S., van Leijen, F., & Hanssen, R. (2025). Peat subsidence and dynamics in Midden-Delfland, the Netherlands, from time series InSAR analysis and the SPAMS model. Geoderma, 463, Article 117551. https://doi.org/10.1016/j.geoderma.2025.117551

Important note

To cite this publication, please use the final published version (if applicable). Please check the document version above.

Copyright

Other than for strictly personal use, it is not permitted to download, forward or distribute the text or part of it, without the consent of the author(s) and/or copyright holder(s), unless the work is under an open content license such as Creative Commons.

Please contact us and provide details if you believe this document breaches copyrights. We will remove access to the work immediately and investigate your claim.

ELSEVIER

Contents lists available at ScienceDirect

Geoderma

journal homepage: www.elsevier.com/locate/geoderma



Peat subsidence and dynamics in Midden-Delfland, the Netherlands, from time series InSAR analysis and the SPAMS model

Yustisi Lumban-Gaol ^{a,b}, Philip Conroy ^a, Simon van Diepen ^a, Freek van Leijen ^a, Ramon Hanssen ^a

- a Department of Geoscience and Remote Sensing, Delft University of Technology, Stevinweg 1, Delft, 2628 CN, The Netherlands
- b National Research and Innovation Agency, Gedung B.J. Habibie, Jl. M.H. Thamrin No. 8, Jakarta Pusat, 10340, Indonesia

ARTICLE INFO

Handling Editor: Budiman Minasny

Dataset link: https://doi.org/10.4121/604b35a 9-8e10-4044-8041-5effacaf6f8a, https://github .com/TUDelftGeodesy/pyspams

Keywords: InSAR Pastures Peatlands SPAMS Subsidence

ABSTRACT

Peat subsidence occurs when parts of the peat soil interact with air, usually due to water table lowering, then triggers peat consolidation, shrinkage, and oxidation, releasing substantial CO2 emissions. Managing and mitigating these impacts requires a comprehensive understanding of the mechanisms and the spatiotemporal variations of the subsidence. Advanced space geodetic techniques, particularly InSAR, enable surface displacement monitoring. While time series InSAR analysis effectively estimates displacement, its precision, accuracy, and representativity are compromised by temporal decorrelation, noise, and dynamic soil movement, especially over pastures on peat soils. Moreover, loss-of-lock events caused by an irrecoverable loss of coherence disrupt the time series and introduce arbitrary unintelligible phase offsets. Strategies such as multilooking using contextual information have improved the reliability of the InSAR displacement estimates. However, more experience in the efficacy of InSAR-based surface dynamics assessments is required. This study estimates and analyzes surface motion in a regional peat area in Midden-Delfland, The Netherlands, using Sentinel-1 data and the SPAMS model. SPAMS incorporates precipitation and evapotranspiration information to estimate surface motion parameters, distinguishing between reversible and irreversible subsidence. The results reveal an average subsidence rate of -5.4 ± 0.7 mm/year within the study area. Irreversible subsidence is strongly correlated with climatic conditions, with the most significant subsidence observed during a prolonged dry period in the summers of 2018 and 2022. Mitigating peatland subsidence includes preserving soil water content, especially during dry periods. Integrating InSAR and SPAMS provides a valuable tool for monitoring peat surface elevation, water management, and reducing peatland degradation.

1. Introduction

A large part of the Netherlands consists of low-lying coastal and fluvial regions characterized by wetlands. It was formed by two geological periods: the Pleistocene glacial activity shaped ice-pushed ridges and sandy plains, and the Holocene sea-level rise created wetter conditions in which peat overtook significant portions of the western and northern Netherlands (Ten Veen et al., 2025). From the Late Iron Age onward, human interaction intensified, accelerating during the medieval period with large-scale reclamation and embankment of coastal and fluvial areas (Borger, 1992; Pierik, 2021). This transformation converted peatlands into polders using dikes and windmills for agricultural and residential use, causing subsidence in drained peatlands.

Lowering of the water table, causing the oxic exposure of organic material in peatlands, results in the processes of peat consolidation, shrinkage, compaction, and CO_2 emission by oxidation, leading into

consequent subsidence (Schothorst, 1982; Hooijer et al., 2011), as illustrated in Fig. 1. Schothorst (1977) found that six years after ditchwater levels had been lowered, surfaces on three polders had subsided 6–10 cm. The study concluded that 65% of it could be attributed to shrinkage and oxidation of organic matter in the layer above the groundwater level. Meanwhile, the rest is expected to be due to the compression of the layer below the groundwater level (Schothorst, 1977). Within approximately 50 years of data, a recent study reports total peat subsidence of 24 and 31 cm, depending on the ditchwater level (Massop et al., 2024).

Addressing the challenges posed by land subsidence in densely populated coastal areas requires a comprehensive grasp of the underlying processes. It includes understanding the factors driving subsidence and their variations across space and time. Leveling can accurately measure surface height differences between benchmarks distributed across the

^{*} Corresponding author at: Department of Geoscience and Remote Sensing, Delft University of Technology, Stevinweg 1, Delft, 2628 CN, The Netherlands. E-mail address: y.a.lumbangaol@tudelft.nl (Y. Lumban-Gaol).

Fig. 1. Conceptual model of peat subsidence processes in drained peatlands. The sequence illustrates the progressive stages of peat subsidence due to drainage: (a) Natural state with intact peat profile; (b) Initial drainage causing decomposition of organic matter and realase of CO_2 ; (c) subsequent subsidence due to compaction and oxidation of peat materials; and (d) Continued drainage leading to a further subsidence and increased CO_2 emissions.

area of interest (Fryksten and Nilfouroushan, 2019). However, existing benchmarks are typically installed in objects with a relatively deep foundation depth and are therefore not sensitive to shallow processes. Installing dedicated benchmarks at the surface in the field is difficult and prone to distortion (Cain and Hensel, 2018; van Asselen et al., 2020), so it is not recommended on a large scale. Furthermore, leveling requires many resources to measure a vast region, including time, human resources, and budget (Saari et al., 2015). Therefore, repeating the measurement in time for elevation monitoring is not efficient.

As an alternative, monitoring land subsidence has been performed using extensometers, which provide precise measurement of vertical displacement at high temporal resolution (Corominas et al., 2000; Liu et al., 2019; Buckley et al., 2003; Miller et al., 2020; Galloway and Burbey, 2011; van Asselen et al., 2020). However, the deployment of extensometers is limited by the high costs associated with their construction and operation, resulting in a sparse network of monitoring stations (Galloway and Burbey, 2011; Maliva and Missimer, 2012; Burbey, 2020). The advent of space geodetic instruments has enabled Earth surface observation without the need for direct field measurements. The repeat period of satellites has the advantage of monitoring the same area periodically. Synthetic aperture radar (SAR), in particular, can be applied to estimate relative elevation changes of the Earth's surface using the interferometric (InSAR) technique (Hanssen, 2001). InSAR performs effectively for objects such as buildings due to their persistent surface characteristics, which ensure consistent radar signal reflections over time. In contrast, applying this technique to areas dominated by vegetation or farmland is more challenging, as the dynamic nature of these surfaces reduces signal coherence (Tampuu et al., 2020; Conroy et al., 2023b; Bhogapurapu et al., 2024).

To address these challenges, InSAR time series analysis has been developed to extract vertical displacement over natural land cover areas such as peat pastures (Morishita and Hanssen, 2015; Alshammari et al., 2018; Tampuu et al., 2020; Liu et al., 2022; Jiang and Lohman, 2021; Conroy et al., 2023b). Nevertheless, the precision, accuracy, and representativity of InSAR in such environments are often compromised by highly dynamic peat soil movement and temporal decorrelation, i.e., the loss of coherence due to changes in the scattering mechanisms over a particular area over time. Moreover, loss-of-lock events caused by an irrecoverable loss of coherence disrupt the time series and introduce arbitrary unintelligible phase offsets (Conroy et al., 2023b). Identifying these events is essential to prevent misinterpretation of phase offsets as displacements. Additionally, ambiguous InSAR observations and imperfect functional models could lead to estimation errors. To mitigate these issues, several strategies have been tested, including multilooking to improve the signal-to-noise ratio (SNR) (Hanssen, 2001; Ferretti et al., 2011; Parizzi and Brcic, 2011; Jiang et al., 2015), selecting only small temporal baseline subsets to reduce decorrelation noise (Berardino et al., 2002; Pepe et al., 2015), and introducing a new functional model called SPAMS (simple parameterization for the motion of soils) by incorporating meteorological data (Conroy et al., 2023b,a). Notably, the latter approach obtained a root mean square difference (RMSD) between InSAR estimates and extensometer measurements in the range of 5-7 mm (Conroy, 2025).

Conventionally, InSAR is used to obtain relative surface elevation changes, which is limited to the period of InSAR data acquisitions. The introduction of the SPAMS model has shifted the focus of InSAR analysis from displacement estimation to the estimation of the driving parameters, which enables forecasting past and future surface motion dynamics. Yet, while the initial studies demonstrating the efficacy of the SPAMS methodology were performed over areas that could be validated with localized multi-year ground truth time series, most areas of interest do not have such extended in-situ infrastructure. Moreover, the main driver of using spaceborne observations lies in the applicability over wide areas, including archive data, and thus the current challenge shifts to those areas, and to alternative means of quality control.

This study evaluates InSAR analysis with the SPAMS model in unsupervised contexts. We analyze relative surface elevation changes in the Midden-Delfland region, the Netherlands, where ground truth is not available. We assess the results through spatio-temporal analysis, considering meteorological data, soil profiles, and elevation. By adopting this approach, this study provides a practical framework for interpreting surface displacement estimates, providing new insights and supporting more informed decision-making where ground truth data are unavailable.

2. Materials and methods

2.1. Study area

The Midden-Delfland region, see Fig. 2, is an open agricultural area with traditional peaty meadows, cows and windmills, used for dairy farming and recreation. It covers an area of $\sim 160~\rm km^2$, with elevations ranging between $-6.4~\rm and + 3~m$ NAP (Dutch ordnance datum). Grasslands or pastures for dairy farming dominate the rural parts, whereas only a few farmlands are used for various crop types, such as corn, wheat, and beets. They are divided into parcels with ditches in between to channel water. These ditches are interconnected within the same water management zone (*peilgebied* in Dutch), where the phreatic groundwater table ($H_{\rm GW}$) within a zone is maintained between certain levels according to the groundwater stages described in de Vries et al. (2003). These stages specify the average highest ($H_{\rm GW,max}$) and lowest ($H_{\rm GW,min}$) groundwater level classes in centimeters below the local ground level (*maaiveld (mv)* in Dutch), thus [cm-mv], i.e., 'centimeters below ground level'. Our study area contains two main classes, i.e.,

- class II: $H_{\rm GW,max}$ < 40 [cm-mv] & 50 < $H_{\rm GW,min}$ < 80 [cm-mv],
- class III: $H_{\rm GW,max} < 40 \ [{\rm cm-mv}] \ \& \ 80 < H_{\rm GW,min} < 120 \ [{\rm cm-mv}].$

Before the wide-scale land reclamation, Midden-Delfland was part of the big Rhine-Meuse delta. These areas now have multi-purpose land use, including agriculture, residential, and recreation. The area is

https://www.pdok.nl/introductie/-/article/basisregistratie-gewaspercelen-brp-

² https://www.ahn.nl

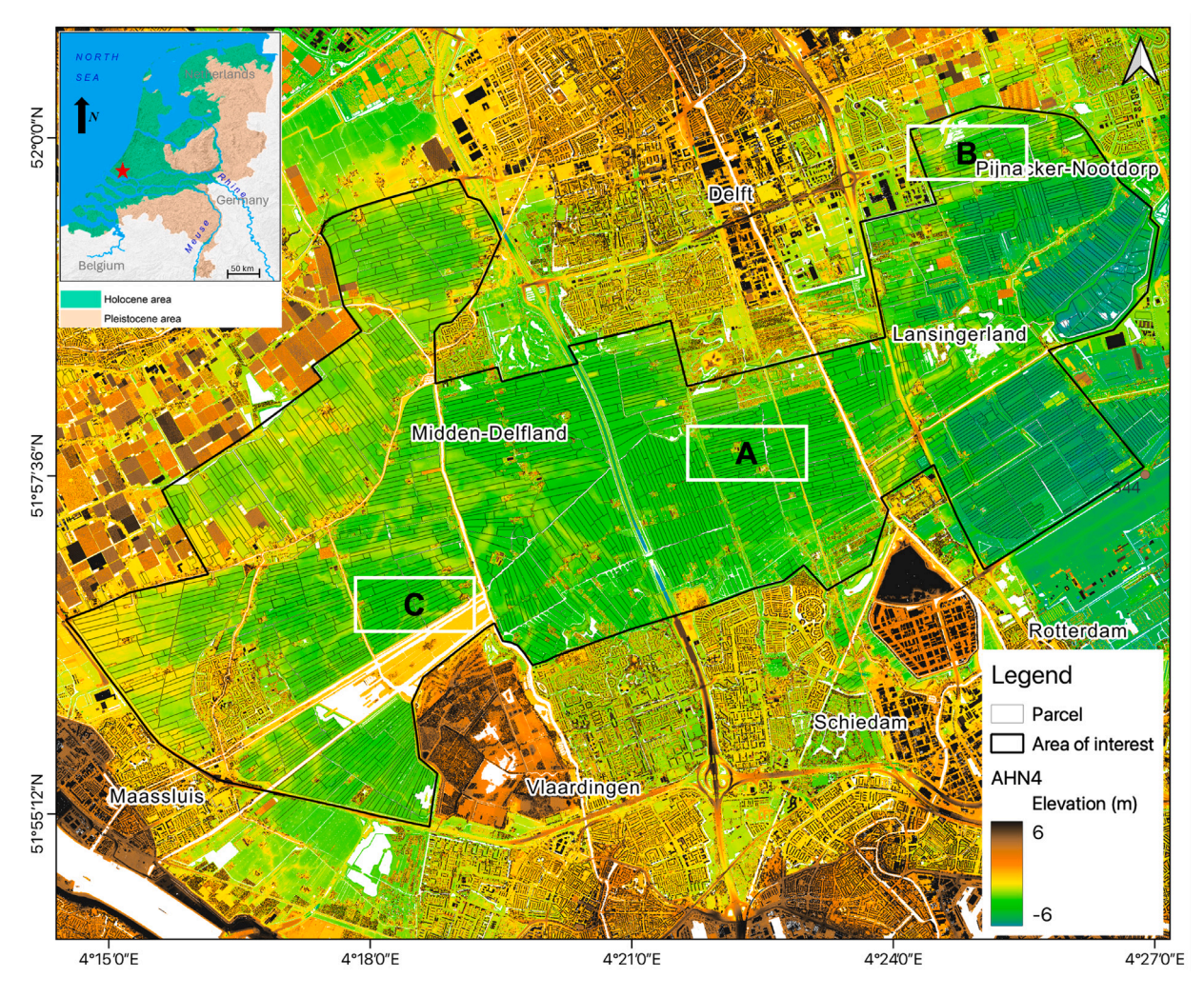


Fig. 2. Midden-Delfland study area overlayed with parcel polygons¹ and surface elevation². The inset map shows an overview of the Holocene and Pleistocene areas within the Netherlands (Van Lanen and Kosian, 2020), where the red star pinpoints our study site. Boxes A, B, and C locate three sample sites for deeper analysis and interpretation, see Figs. 3–5.

characterized by substantial peat and clay deposits, with an average peat thickness of approximately 1–3 m. In the eastern part of the research area, peat thickness can exceed 3 m, although some sections are dominated by clay soils. In the central region, peat thickness ranges from 1 to 3 m. In contrast, the western area has peat thicknesses of less than 1 m, with clay predominating in the soil composition. These values represent the total thickness within a 50 m soil profile, as indicated by the TNO Geological Survey model³.

Given the geological formation and reclamation history of this dynamic Holocene region — where much of the land was drained and converted into pasture, alongside typical wetland conditions — it is crucial to understand the long-term subsidence resulting from peat cultivation. This understanding is especially important for government decision-making and the implementation of effective adaptation measures to address the persistent challenges associated with land subsidence.

2.2. Data

We used SAR observations from the Sentinel-1A/B satellites using the interferometric wide swath (IW) mode and a single VV polarization. These satellites operate in C-band with a 12-day repeat period. When

Table 1 Summary of SAR Sentinel-1 data from January 2016 to December 2024.

Orbit	Track number	Number of acquisitions			
Ascending	88	406			
	161	424			
Descending	37	419			
	110	426			

combined, the two-satellite constellation provides a six-day repeat cycle. Our dataset includes data from four orbit tracks: two descending tracks (37 and 110) and two ascending tracks (88 and 161), see Table 1. Collectively, these tracks yield a high revisit rate of 1 – 3 days. We analyzed a total of 1675 acquisitions spanning from 1 January 2016 to 31 December 2024, considering both descending and ascending observations. All single look complex (SLC) SAR images were coregistered and geolocated using the Doris software (Kampes and Usai, 1999; Kampes et al., 2004; Arikan et al., 2008).

Observations from satellite images were enriched with geospatial contextual information, as listed in Table 2. It includes parcel, soil, water table, and meteorological data, which are used during InSAR processing. Parcel, soil, and water table are vector datasets available through the Netherlands geospatial database website. Parcel data provides information on crop type and parcel geometry, while the soil map describes the spatial distribution of soil types and key soil profile

³ https://www.dinoloket.nl/ondergrondgegevens

List of contextual information used in the relative surface elevation changes analysis.

Data	Information	Source	Data Type
Parcel	Parcel geometry, crop type	PDOK-BRP	Vector polygon
Soil	Shallow soil type (< 1.2 m depth)	PDOK-BRO	Vector polygon
Water table	Water table zone	PDOK-Peilgebied	Vector polygon
Meteorological	Precipitation, evapotranspiration	KNMI	Vector point and tabular
Elevation	Terrain elevation	AHN	Raster 0.5×0.5 m
Lithology	Soil class per 50 cm from the surface	DINOloket	Vector point
	down to a depth of 50 m		

characteristics to a depth of 1.2 m. Water table data specifies zones where parcels share the same groundwater table. Meteorological data from the Royal Netherlands Meteorological Institute (KNMI) include daily precipitation and evapotranspiration records from their stations. To assign unique attributes of soil type and water table zone, a spatial join with a one-to-one relationship was performed, retaining only the attributes of the feature with the largest overlap. For meteorological data, the closest station within a maximum distance of 15 km from the parcel centroid was selected. In addition to these datasets, elevation and lithology data are used to analyze the results. The elevation model is derived from airborne laser scanning data acquired in 2022 and is provided in raster format with a resolution of 50 cm. Lithology data from the TNO Geological Survey model the lithology type for each 50 cm increment from the surface down to a depth of 50 m.

2.3. InSAR parameter estimation with the SPAMS model

Time series analysis of InSAR has been performed to model ground motion using a stack of SAR data in the same area. The coherence level plays an important role in determining how many targets can be detected for analysis. Two classes of targets can be distinguished based on their scattering mechanisms: point scatterers (PS) and distributed scatterers (DS) (Hu et al., 2019). PS targets appear when a strongly reflecting object dominates the pixel in each radar image in the stack, which usually comes from man-made features in the built environment. On the other hand, DS occur when many small objects contribute to the pixel reflection. They often correspond to natural targets, such as bare or vegetated surfaces, which exist primarily in rural regions. Since our focus is on peatland displacement, this study used the InSAR DS parameter estimation workflow as implemented in DECADE (TU Delft, 2024). For comprehensive methodological details, readers are referred to Conroy (2025). Here, we briefly outline the key aspects relevant to the analysis.

Three main steps are necessary to retrieve relative elevation changes from InSAR observations. First, parcel-based multilooking was performed using the coregistered SAR stack to estimate the coherence matrix from all possible interferometric combinations. Based on this matrix, the Eigendecomposition-based Maximum-likelihood-estimator of Interferometric phase (EMI) (Ansari et al., 2018) was applied, reducing the complete set of interferometric combinations to a single set of phases. The results are equivalent to when computing interferometric combinations with one reference image (Samiei-Esfahany et al., 2016). Subsequently, each parcel was treated as a virtual PS, represented by its centroid, and integrated with available PS within the study area for atmospheric phase screen filtering. This process results in a set of observed phases for each track.

Loss-of-lock events, which occur during incoherent periods, causing gaps within the time series data. These events introduce an unknown vertical displacement that is specific to each parcel and observation epoch. To address this, we employed the SPAMS (Simple Parameterization for the Motion of Soils) model developed by Conroy et al. (2023a). SPAMS estimates surface motion parameters based on physical processes and distinguishes between reversible and irreversible subsidence. The model uses precipitation P(t) and evapotranspiration E(t)data from nearby meteorological stations, assuming that these factors

primarily drive soil movement. The model is expressed as (Conroy et al., 2023a):

$$H(x, P(t), E(t)) = \underbrace{\left[\sum_{t} (x_{P}P(t) - x_{E}E(t))\right] + \left[\sum_{-\infty}^{t} x_{I} \cdot f(x, P(t), E(t))\right],}_{\text{reversible}}$$
 (1)
$$\text{where } f(x, P(t), E(t)) = \begin{cases} 0, & \text{for reversible} > 0.\\ 1, & \text{for reversible} \leq 0. \end{cases}$$
 (2)

where
$$f(x, P(t), E(t)) = \begin{cases} 0, & \text{for reversible} > 0. \\ 1, & \text{for reversible} \le 0. \end{cases}$$
 (2)

SPAMS includes four parameters: (i) the scaling factor of precipitation $x_{\rm P}$, (ii) the scaling factor for evapotranspiration $x_{\rm E}$, (iii) the integration time τ in days, and (iv) the subsidence rate x_I in mm/day. The first two contribute to the reversible component (e.g., shrinkage and swell), with the integration time representing the accumulation time or latency of the reversible effects. The last parameter x_1 represents the irreversible component (e.g., oxidation) and is assumed to be only active during dry periods, i.e., when evapotranspiration exceeds precipitation (ibid.).

The SPAMS model becomes the functional model used in the final step, focusing on estimating displacement model parameters as well as the phase ambiguities. The estimation was performed on both parcelbased and group-based levels. Initially, the segmented phase time series per parcel, along with a set of initial displacement parameters, were used to optimize the SPAMS model parameters. The segmentation is based on the coherence threshold and the number of consecutive observations exceeding that threshold. Specifically, a coherence threshold of 0.19 with a minimum of five consecutive epochs above this threshold was used.

Following per-parcel estimation, displacement parameters, particularly $x_{\rm I}$, were re-estimated for contextually homogeneous groups of parcels, assuming that parcels within the same category behave similarly (Conroy et al., 2023b). The grouping is necessary to address lossof-lock events between parcels due to temporal decorrelation, thereby reducing segment shift noise, which occurs more frequently when only using per-parcel observations. This contextual group was determined based on the land cover, soil type, and groundwater management zone. Here, we only include grassland parcels to avoid non-Lagrangian processes due to crop cycles and ploughing. We only include parcels that can form a group with a minimum of ten parcels.

In both procedures, the unknown shift between segments as well as the integer phase ambiguity were estimated using the displacement model, facilitating the phase ambiguity resolution and reconnection of observations. Finally, the final displacement model was then fitted to the unwrapped phase data, projected onto the vertical, and used to estimate a set of final displacement parameters for each parcel. The estimated model parameters were used to generate realizations of relative elevation changes using Eqs. (1) and (2), with daily precipitation and evapotranspiration as inputs.

To evaluate model suitability and identify whether an error is present in the mathematical model, the $\hat{\sigma}^2$ -statistic is computed based on the weighted sum of squared residuals between InSAR and SPAMS, normalized by the degrees of freedom for each parcel (Teunissen, 2024). Values close to one suggest model adequacy, while values larger than one indicate either model imperfections or an overly optimistic stochastic model. Conversely, values significantly smaller than one imply either an overly pessimistic stochastic model, i.e., underestimating the quality of observations, or an over-parameterized functional model.

Table 3 Estimated displacement model parameters $(x_p, x_E, x_I, and \tau)$ with its uncertainty (1-sigma), $\hat{\sigma}^2$ -statistic , number of InSAR data above the specified threshold used during the estimation process (N_{obs}) , estimated annual irreversible rate (v_I) , and contextual information for each parcel at Sites A, B, and C. Soil codes are elaborated in Table 4.

Location	Area	Soil	$x_{\rm P}$	$x_{\rm E}$	$x_{\rm I}$	τ	$\hat{\sigma}^2$ -	$N_{ m obs}$	v_{I}
	m ²	code ^a			(mm/day)	(days)	statistic		(mm/y)
Site A									
Parcel a	12,793	hVc	0.070 ± 0.003	0.106 ± 0.004	-0.0279 ± 0.0007	74	0.75	375	-5.0
Parcel b	19,110	hVc	0.068 ± 0.003	0.159 ± 0.004	-0.0265 ± 0.0006	70	0.87	429	-5.9
Parcel c	18,673	hVc	0.071 ± 0.003	0.173 ± 0.004	-0.0270 ± 0.0006	70	0.77	443	-6.1
Parcel d	15,254	hVc	0.071 ± 0.003	0.204 ± 0.005	-0.0272 ± 0.0005	70	0.85	428	-6.5
Site B									
Parcel a	21,970	Mv41C	0.070 ± 0.002	0.112 ± 0.003	-0.0256 ± 0.0005	69	0.91	579	-4.8
Parcel b	18,908	kVc	0.071 ± 0.002	0.150 ± 0.003	-0.0280 ± 0.0004	70	1.09	585	-6.0
Parcel c	9,343	kVc	0.068 ± 0.003	0.097 ± 0.003	-0.0278 ± 0.0005	70	1.15	355	-4.9
Parcel d	17,035	kVc	0.070 ± 0.002	0.121 ± 0.003	-0.0266 ± 0.0004	70	0.96	616	-5.2
Site C									
Parcel a	38,025	hVd	0.070 ± 0.002	0.153 ± 0.003	-0.0286 ± 0.0004	67	1.03	657	-6.2
Parcel b	16,092	Wo/pMn85C	0.072 ± 0.003	0.166 ± 0.002	-0.0275 ± 0.0004	68	1.09	552	-6.1
Parcel c	35,062	Wo/pMn85C	0.066 ± 0.002	0.118 ± 0.002	-0.0263 ± 0.0004	71	1.01	625	-5.3
Parcel d	9,688	hVd	0.074 ± 0.003	0.109 ± 0.003	-0.0303 ± 0.0007	70	1.10	377	-5.4

^a https://legenda-bodemkaart.bodemdata.nl/bodemclassificatie.

3. Results and discussion

3.1. Estimated time series surface displacements

This study estimates a time series of relative surface elevations for 1127 parcels covering Midden-Delfland using InSAR data from 1 January 2016 to 31 December 2024. To illustrate soil motion variability within our study area, cross sections of three locations (see boxes on Fig. 2) were generated, together with the estimated time series surface motion at the parcel level. Additionally, we present sample soil profiles within each parcel based on the lithology data, showing that peat, clay, and sand materials are present within the soil profiles at these three locations.

Figs. 3–5 provide a comprehensive overview of Site A, B, and C, respectively, each displaying parcel shapes and sizes overlay on elevation models, cross-section elevation profiles and water table configurations, modeled surface motion time series, and sample-based subsurface lithology. Across all sites, the elevation profiles indicate generally uniform terrain, except for parcels B.a and C.c, where an elevation inversion is observed. The elevation model suggests that these elevated areas were originally riverbeds, but prolonged land subsidence has altered this condition, causing the riverbed to become elevated relative to the surrounding terrain. Parcels with this type of terrain typically have mixing of soil types, which impacts the representability of the estimated displacement parameters.

Within this context, Site A presents results from parcels belonging to a single contextual group, all classified as cultivated peat soils and share the same water management zone. As shown in Table 3, the displacement parameter estimates for these parcels are comparable, except for the scaling factor for evapotranspiration $x_{\rm E}$, which is lowest for parcel A.a. It suggests that, given equivalent precipitation and evaporation, parcel A.a is less susceptible to precipitation deficit, resulting in a lower annual subsidence rate $(v_{\rm I})$ —approximately 1 mm/year less than the other parcels. Soil mapping further reveals that, unlike the other parcels, the western portion of parcel A.a consists of a mix of chalk-poor sea clay or boggy soil and clay. The presence of different soil types within parcel A.a may explain its different behavior compared to neighboring parcels.

In contrast, parcel A.d exhibits an annual subsidence rate 0.5 mm/ year higher than parcel A.b and A.c, attributed to its exposed peat top layer, which makes it more prone to rapid oxidation than neighboring parcels covered by clay or sand. This pattern of subsidence associated with exposed organic layers is likewise observed at Site B, where parcel B.b lacks clay cover despite having the same soil classifications as its adjacent parcels. Consistently, both parcel A.d and B.b have

larger scaling factors for evapotranspiration, resulting in higher annual subsidence rates than the surrounding peat parcels.

While Site A and B represent a group of peat parcels situated next to each other, Site C is differentiated by the presence of two peat parcels, C.a and C.d, separated by peaty/clay parcels in between. Although the initial hypothesis considered that surface motion within a group would be comparable, analysis of the estimated surface motion time series reveals otherwise: parcel C.a shows displacement patterns similar to C.b, as do parcels C.c and C.d, despite differences in soil type and water management. Soil mapping clarifies that the western section of parcel C.d shares the same soil types as parcel C.c, likely explaining its similarity in displacement behavior to parcel C.c than C.a. Similar soil mixing also occurs in parcel C.b, where parts of it have the same soil class as C.a.

The estimated time series surface displacement at these three sites indeed suggests a correlation with meteorological data, revealing a consistent seasonal pattern: winter uplift is driven by precipitation surplus and reduced evapotranspiration, while summer subsidence is caused by water deficit. The oscillations between the summer and winter periods typically range in magnitude from ~30 to 50 mm. Extreme drought events, such as those in 2018 and 2022, amplified these dynamics, causing subsidence peaks of ~50 to 70 mm over six months. This subsidence peak strongly coincides with periods of very low rainfall and high evapotranspiration compared to other years.

Additionally, Table 3 depicts the $\hat{\sigma}^2$ -statistic across all parcels for these three sample sites, which range between 0.75 and 1.15. The upper bound falls slightly above 1, which could indicate minor model fit incompatibility or slightly overestimated measurement uncertainties, while the lower bound reflects a moderate estimate of observational uncertainty. Yet, both extremes remain within a reasonable range. Although these site-specific results indicate no significant evidence of model deficiencies or errors, the overall $\hat{\sigma}^2$ -statistic across the study area exceed these intervals, which is analyzed further in Section 3.4.

3.2. Implications

Interactions between soil composition, hydrological parameters, and elevation-driven exposure primarily drive the variability in surface displacement rates among parcels with similar contextual conditions. Assigning unique soil type attributes to each parcel by retaining the attributes from the largest overlap during the spatial join results in mixed soil types within a parcel, which in turn affects the estimation and interpretation. Further algorithm adjustments could involve intersecting soil map boundaries with parcel geometries to partition mixed soil areas. However, this approach risks reducing multilooking quality

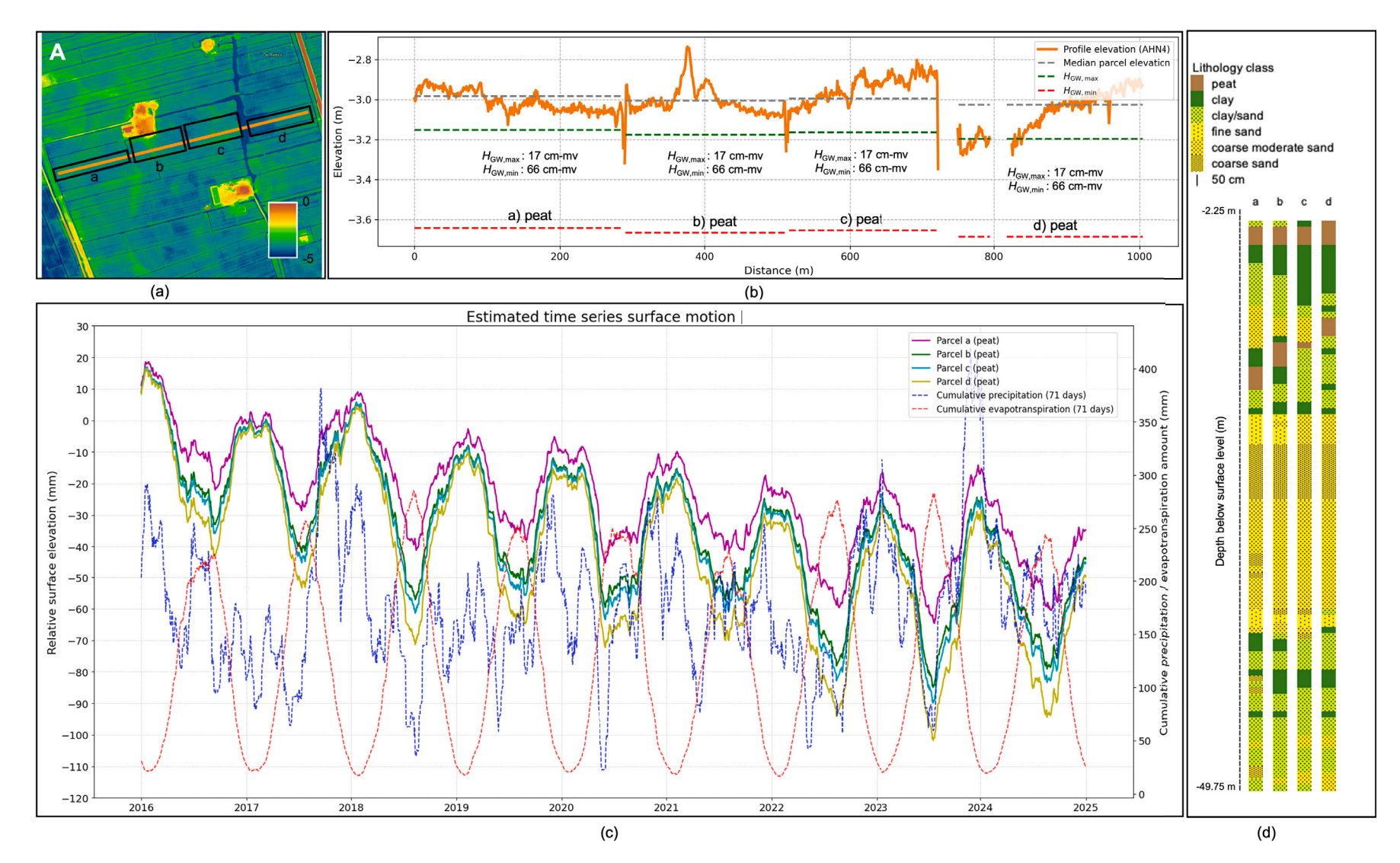


Fig. 3. The overview of Site A includes the elevation model and parcel geometry (a), the cross-section profile of the parcels showing surface elevation and water table level setup (b), the estimated time series of surface motion from the SPAMS model together with cummulative precipitation and evapotranspiration (c), and sample lithology layers, illustrating subsurface composition (d).

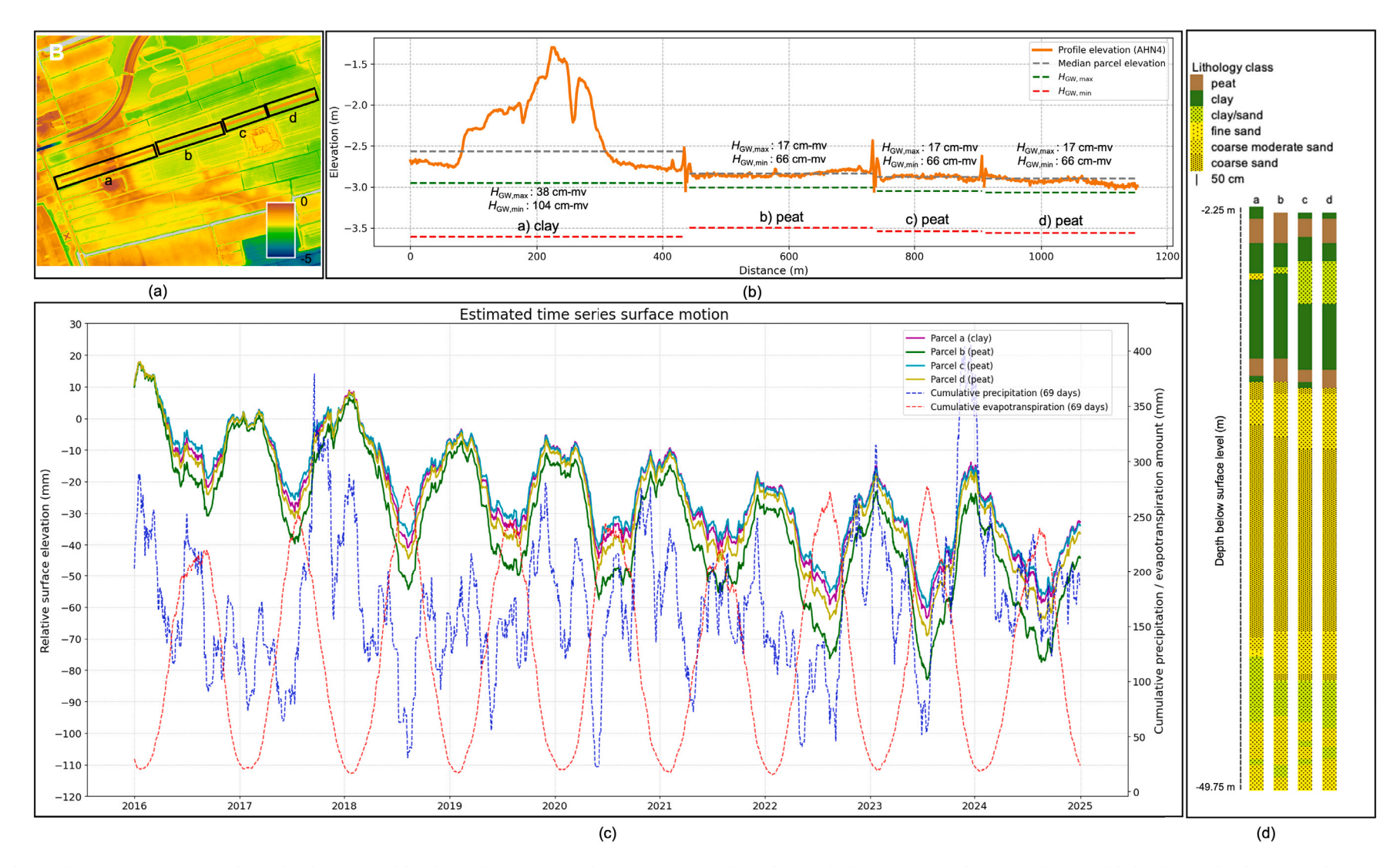


Fig. 4. The overview of Site B includes the elevation model and parcel geometry (a), the cross-section profile of the parcels showing surface elevation and water table level setup (b), the estimated time series of surface motion from the SPAMS model together with cummulative precipitation and evapotranspiration (c), and sample lithology layers, illustrating subsurface composition (d).

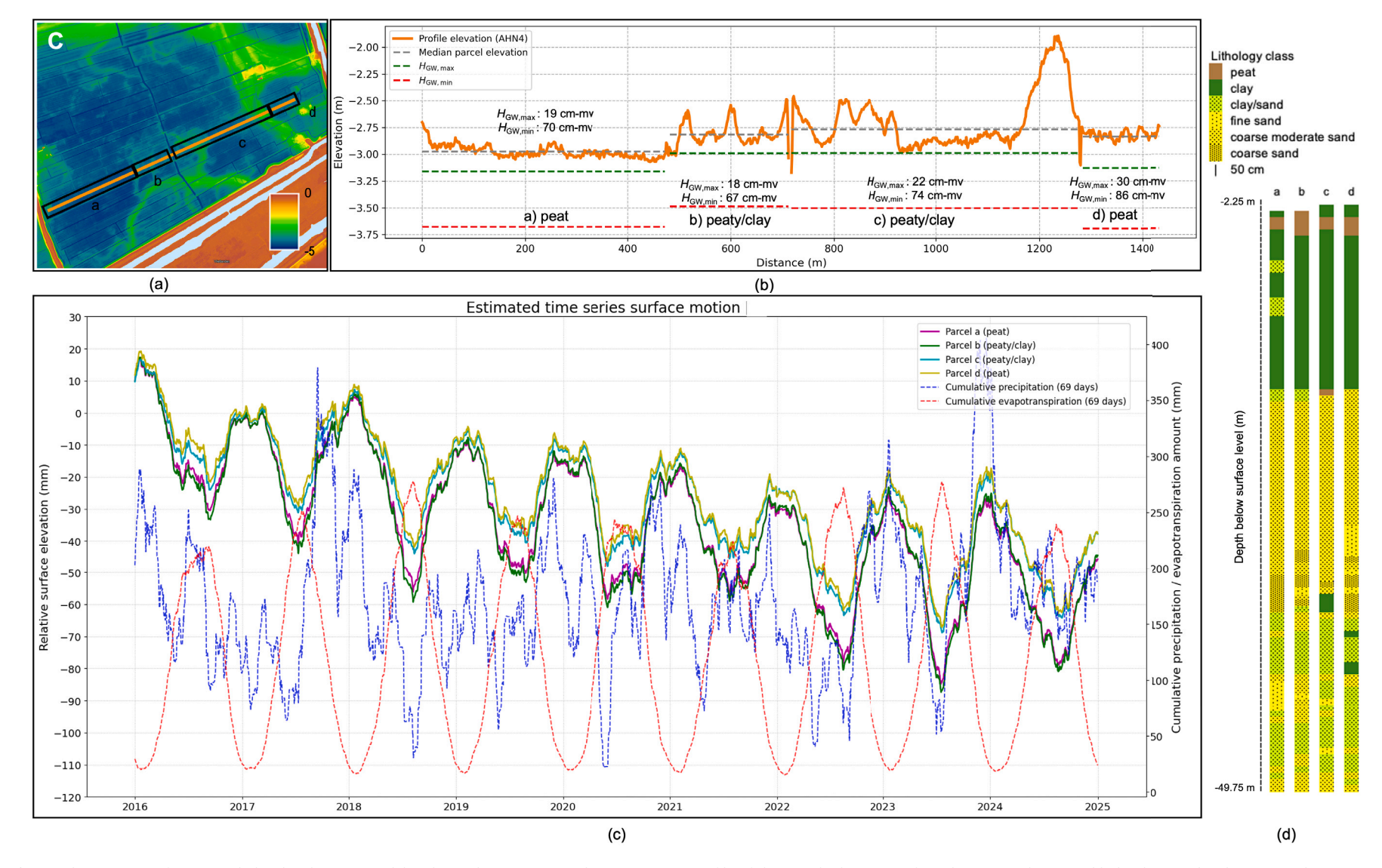


Fig. 5. The overview of Site C includes the elevation model and parcel geometry (a), the cross-section profile of the parcels showing surface elevation and water table level setup (b), the estimated time series of surface motion from the SPAMS model together with cummulative precipitation and evapotranspiration (c), and sample lithology layers, illustrating subsurface composition (d).

Table 4
Soil code taxonomy, based on Dutch soil classification system, and their interpretation (de Bakker and Schelling, 1989

Soil code ta	xonomy, based on Dutch soil classification system, and their interpretation (de Bakker and Schelling, 1989).
hVc	Dutch: "Koopveengronden op zeggeveen, rietzeggeveen of (mesotroof) broekveen"
	Cultivated peat soils (former natural peat soils that have been reclaimed and used for agriculture or other human
	purposes) on sedge peat (Peat formed mainly from sedges, i.e., Carex species), reed-sedge peat (peat composed of
	a mixture of reeds (Phragmites) and sedge vegetation) or (mesotrophic) fen peat ("broekveen" refers to fen peat,
	typically found in low-lying areas; mesotrophic indicates a moderate nutrient status).
kVc	Dutch: "Waardveengronden op zeggeveen, rietzeggeveen of (mesotroof) broekveen"
	Low peat soils (i.e., peat soils that have subsided significantly due to drainage, oxidation, and agricultural use,
	typically found in low-lying floodplains or reclaimed peat areas.) on sedge peat, reed-sedge peat or
	(mesotrophic) fen peat.
hVd	Dutch: Koopveengronden op bagger, verslagen veen, gyttja of andere veensoorten
	Cultivated peat soils on dredged material ("bagger" refers to soft, organic-rich sediment often found in drained or
	dredged water bodies), decomposed peat (highly degraded or amorphous peat, where original plant structures are
	no longer recognizable due to decomposition), gyttja (a fine, organic-rich sediment formed in freshwater lakes,
Mv41C	composed of decomposed aquatic organisms and mineral matter) or other types of peat. Dutch: Kalkarme drechtvaaggronden in zeeklei, zware klei, profielverloop 1
WV41C	Calcium-poor (soils with low calcium carbonate content) dredged vaag soils ("vaaggronden" are young, weakly
	developed mineral soils with limited horizon development. The prefix "drecht" indicates formation under influences
	of water management or dredging, typically in reclaimed or modified landscapes) developed in marine clay (clay
	deposited in a marine (i.e., saltwater) environment, common in the Dutch coastal plains) (heavy clay: clay soils
	with a high percentage of fine particles, making them dense and difficult to work), profile type 1 (a classification
	referring to the vertical development of the soil profile; in this case, a very weakly developed profile with minimal
	horizon differentiation).
Wo	Dutch: Plaseerdgronden; gronden met een moerige bovengrond of moerige tussenlaag op niet-gerijpte zavel of klei
	Plaseerd soils (a Dutch soil type term used in soil classification for transitional soils, often found in areas with
	artificial drainage or sedimentation. The term is often kept untranslated in scientific Dutch-English contexts, but
	can be described as "transition soils with peaty layers over young mineral material.); soils with a peaty topsoil
	("Moerig" refers to a top layer that contains a significant proportion of partially decomposed organic matter, i.e.,
	peat-like) or peaty interlayer (an organic-rich layer within the soil profile, not necessarily at the surface) over
	unripe loam or clay ("unripe" refers to young, water-saturated, unconsolidated mineral soil that has not yet
	undergone 'ripening'—a process of soil structure development and consolidation).
pMn85C	Dutch: Kalkarme leek-/woudeerdgronden in zeeklei, klei, profielverloop 5
	Calcium-poor leek/woudeerd soils (a compound term combining two Dutch soil classifications: (i) leekeerdgronden,
	i.e., soils influenced by drainage, often in marine clay, typically developed under grassland, and (ii)
	woudeerdgronden, i.e., similar soils developed under forest or woodland. Together, these are ripened marine clay
	soils with significant profile development, often influenced by long-term land use, i.e., grassland or forest) in marine clay (Soils developed in marine-deposited clay, typically heavy in texture), profile development 5
	(indicates strongly developed soil horizons, often with clear differentiation and structure due to long-term
	soil-forming processes).
	son-torning processes).

due to fewer number of looks within smaller parcel sizes. This tradeoff highlights the importance of balancing spatial resolution and data reliability in heterogeneous soil environments.

Sensitivity to subsidence is influenced by differences in soil layering, such as the presence or absence of clay or peat at the surface. Even when slight, elevation differences alter the extent of peat surface exposure to air, thereby influencing oxidation and subsidence rates. Querner et al. (2008) recommends that water management focus on methods to keep the water level in summer as high as possible to reduce the subsidence rate. Soil stratigraphy further contributes to differential responses among parcels. As demonstrated by Brouns (2016), peat soils lacking clay covers are more prone to accelerated subsidence due to increased oxygen intrusion and oxidation. The clay layers reduce water deficit susceptibility by maintaining higher soil saturation. As described in Section 3.1, the estimated SPAMS parameters, particularly the scaling factor for evapotranspiration $x_{\rm E}$, clarify these mechanisms by affecting precipitation deficit sensitivity and the timescale of reversible displacement. Parcels with clay covers exhibit lower x_E values, reflecting reduced sensitivity to evapotranspiration-driven water loss.

In contrast, bare peat parcels exhibit higher $x_{\rm E}$ values, amplifying evapotranspiration effects and accelerating reversible shrinkage. This trend aligns with findings by Van Den Akker et al. (2012), where parcels with a clay layer on top showed reduced subsidence levels compared to bare peat, as clay impedes drainage and maintains higher soil saturation. The water-retention properties of clay can clog water drainage, keeping the overlying peat more saturated and thereby reducing peat consolidation (Dawson et al., 2010). Collectively, these findings underscore the necessity of integrating both spatial and temporal factors — soil lithology, SPAMS parameters, elevation gradients, and meteorological extremes — into predictive models for land subsidence. Such holistic approaches enable targeted management strategies for site-specific geotechnical heterogeneity and climatic variability.

3.3. Estimated linear subsidence rates

Linear subsidence rates are estimated by least squares on the results. Fig. 6 displays the spatial distribution of these rates, ranging from $-2.3\,$ mm/year to $-8.2\,$ mm/year, with an overall mean subsidence of $-5.4\pm0.7\,$ mm/year for the region. These ranges are comparable with findings from other studies on peatlands in other regions within the Netherlands, such as -5 to $-10\,$ mm/year near Gouda (Conroy et al., 2024) and $-8\,$ mm/year in the polder near Amsterdam (Hoogland et al., 2012). Similar subsidence rates are also observed in neighboring countries characterized by peatlands, including Sweden (-5 to $-25\,$ mm/year) (Berglund and Berglund, 2010) and Norfolk, UK (-9 to $-18\,$ mm/year) (Dawson et al., 2010).

3.4. SPAMS parameters and estimation quality

Excluding the cropped parcels, approximately 68% of parcels are included in the analysis, while the remaining 32% are omitted due to insufficient neighboring parcels to form contextual groups. The heterogeneous distribution of soil types within the study area complicates the identification of parcels with similar soil characteristics and groundwater management zones, resulting in contextual groups of only 5–7 parcels. Temporal data gaps from loss-of-lock events are mitigated using neighboring parcel data within the same group. However, groups with fewer than ten parcels are inadequate for reliable analysis. With a minimum of ten parcels per contextual group, SPAMS parameters exhibit spatial variability, see Fig. 7a–c, with ranges of 0.060–0.132 $(x_{\rm P})$, 0.093–0.294 $(x_{\rm E})$, and –0.031 to –0.0234 $(x_{\rm I})$, and medians of 0.070, 0.116, and –0.0273, respectively.

These parameters enable subsidence prediction under consistent contextual conditions and estimate peat volume loss due to subsidence

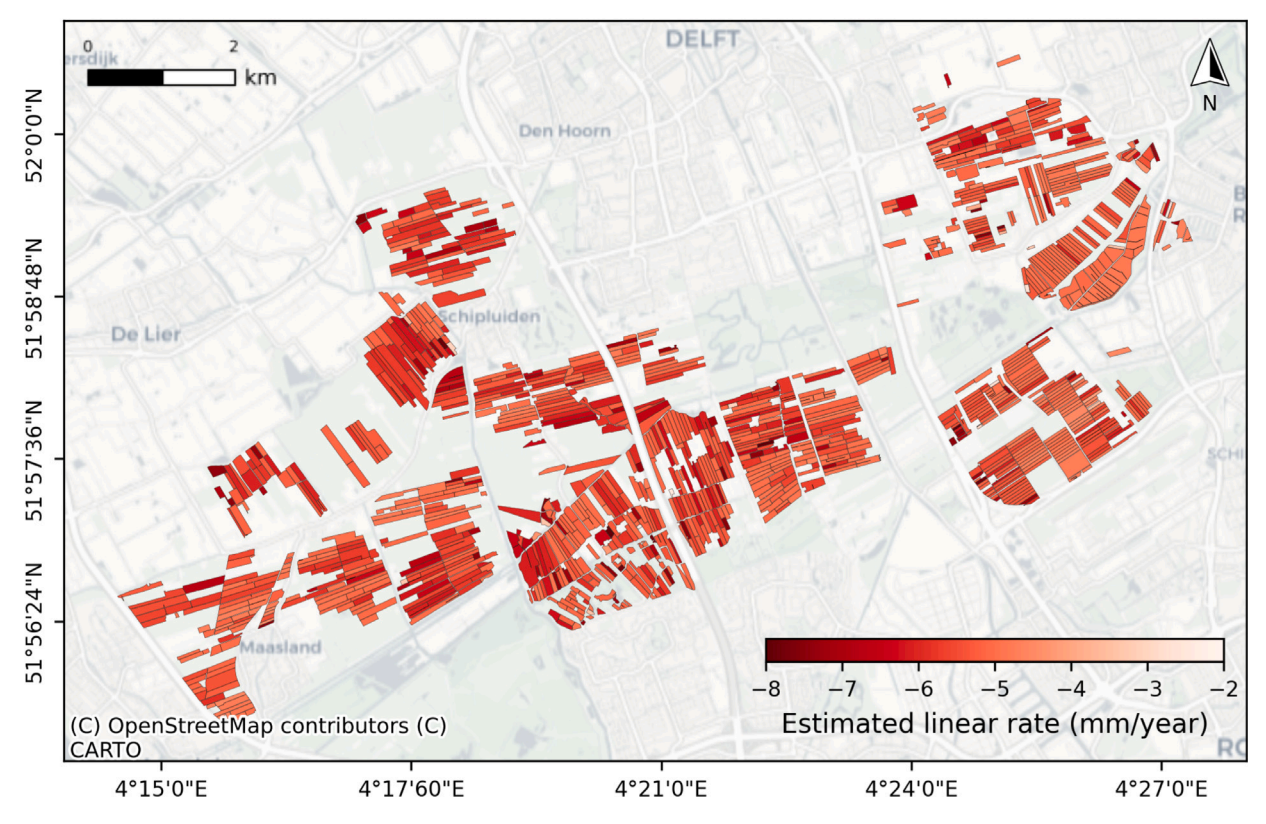


Fig. 6. Estimated linear subsidence rates in Midden-Delfland shows the spatial distribution ranging from -2.3 to -8.2 mm/year, with an overall mean subsidence of -5.4 ± 0.7 mm/year.

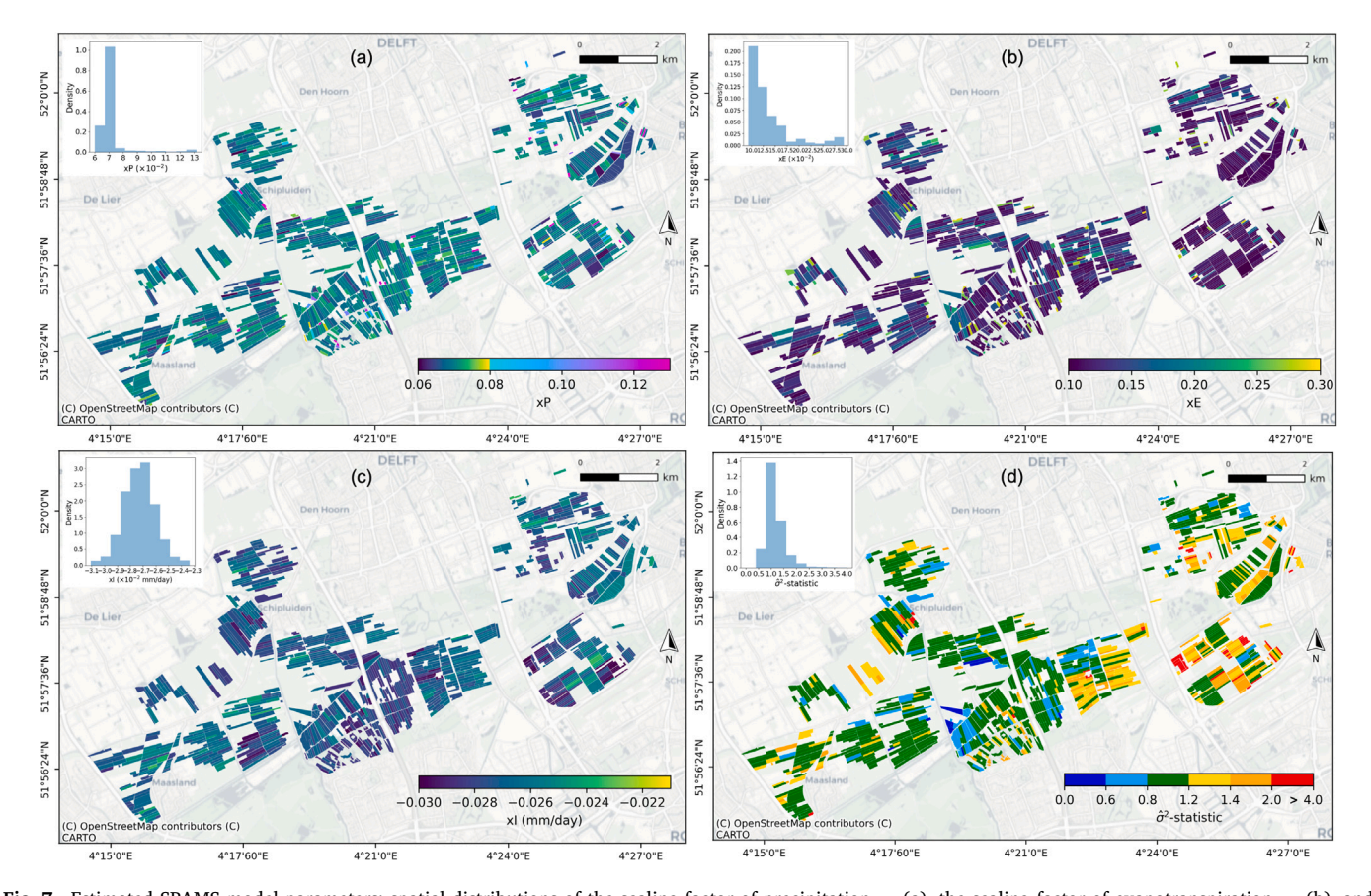


Fig. 7. Estimated SPAMS model parameters: spatial distributions of the scaling factor of precipitation $x_{\rm P}$ (a), the scaling factor of evapotranspiration $x_{\rm E}$ (b), and the subsidence rate $x_{\rm I}$ in mm/day (c) highlight regional variability. Panel (d) shows the distribution of the $\hat{\sigma}^2$ -statistic, with values around '1' indicating generally good model performance across most parcels.

associated with the irreversible component. The SPAMS model suggests that irreversible subsidence is directly linked to climatic conditions. The average annual irreversible contribution to total subsidence reveals that parcels subside more in certain years, particularly during drought episodes, such as the prolonged dry period in 2018 and 2022. A comparison between mean annual irreversible subsidence and annual SPEI (standardized precipitation evapotranspiration index) (Vicente-Serrano et al., 2010) yields a Pearson correlation of 0.79 with a *p*-value of 0.01. The annual SPEI from 2016 to 2024 remains within the normal range (indices between –1 and 1), except for 2018 and 2022, which display values of –2.3 and –1.4, indicating extremely and moderately dry conditions, respectively. These findings enhance our understanding of climate-peatland-water system interactions and subsidence dynamics.

The SPAMS displacement model parameters are designed to capture local water balance processes, including soil infiltration, groundwater storage, and transpiration, in relation to surface height variations. Notably, when the scaling factor for evapotranspiration is higher than precipitation, it suggests that irreversible processes dominate when precipitation is approximately equal to or less than the amount of evapotranspiration. It is important to acknowledge that the model estimation relies on meteorological data from a station $\sim 3-15$ km away, so irregular conditions within the study area may not be observed and affect the accuracy of its estimates.

The SPAMS model currently takes precipitation and evapotranspiration data to represent the in- and out-flow of water. This approach, while accounting for natural hydrological processes, does not fully capture the complexity introduced by drainage systems through the pumping of water in or out of ditches. Despite the relatively rapid nature of these drainage processes, the potential effects of such pumping activities on surface motion dynamics require further investigation to ensure comprehensive model accuracy.

Additionally, the calculated $\hat{\sigma}^2$ -statistic as in Fig. 7d ranges from 0.45 to 9.04, where larger values are primarily located in the eastern part of the study area. These are the locations where former peat extraction zones are identified based on the elevation data. Values larger than 2.0 are associated with outliers from low coherence thresholds. Meanwhile, values between 1.2 and 2.0 predominantly occur in natural grassland parcels with agricultural functions, distinct from permanent grasslands, warranting further investigation.

4. Conclusions

This study comprehensively assesses relative surface elevation changes across 1127 parcels in Midden-Delfland from 2016 to 2024, utilizing InSAR data and contextualized by detailed soil, lithology, and water management information. The analysis demonstrates that the soil composition, hydrological parameters, and elevation-driven exposure primarily drive spatial and temporal variability in surface displacement. Notably, the presence or absence of clay layers, subtle elevation differences, and parcel-specific SPAMS model parameters collectively influence the rates and mechanisms of subsidence. Seasonal oscillations in surface elevation during drought periods amplify subsidence rates. The observed linear subsidence rates, averaging -5.4 ± 0.7 mm/year, are consistent with findings from other peatland regions in the Netherlands and neighboring countries, underscoring the broader applicability of these results.

The SPAMS model effectively captures local water balance processes and their impact on surface elevation dynamics despite limitations related to meteorological data resolution and contextual group size. $\hat{\sigma}^2$ -statistics further support the model's adequacy for most parcels, though some variability remains in areas with low coherence or distinct land use. Importantly, the irreversible component of subsidence is closely linked to climatic extremes, particularly during drought episodes, highlighting the vulnerability of peatlands to ongoing climate variability. These findings emphasize integrating soil stratigraphy, hydrological

management, and climatic data into predictive models to inform targeted subsidence mitigation strategies. Overall, this work advances understanding of the complex interactions between climate, soil, and water management in driving peatland subsidence, providing a foundation for improved land and water resource management in vulnerable lowland regions.

CRediT authorship contribution statement

Yustisi Lumban-Gaol: Writing – original draft, Visualization, Validation, Formal analysis, Data curation, Conceptualization. Philip Conroy: Writing – review & editing, Software, Methodology. Simon van Diepen: Software. Freek van Leijen: Writing – review & editing, Supervision, Software, Formal analysis. Ramon Hanssen: Writing – review & editing, Validation, Supervision, Formal analysis, Conceptualization.

Declaration of competing interest

The authors declare that they have no known competing financial interests or personal relationships that could have appeared to influence the work reported in this paper.

Acknowledgments

This research is supported by the Indonesian Endowment Fund for Education (LPDP) and satellite data from the European Union's Copernicus program. The authors would like to thank Sipke Riemersma and Peter Hollanders of the Delfland Regional Water Authority for their support in the initial stages of this study.

Data availability

The estimated displacement parameters dataset over the study area is available through the 4TU.ResearchData repository: https://doi.org/10.4121/604b35a9-8e10-4044-8041-5effacaf6f8a (Lumban-Gaol and Hanssen, 2025). The dataset is compatible with open-source geospatial analysis tools and can be readily imported into Python-based workflows using the pyspams library: https://github.com/TUDelftGeodesy/pyspams.

References

Alshammari, L., Large, D.J., Boyd, D.S., Sowter, A., Anderson, R., Andersen, R., Marsh, S., 2018. Long-term peatland condition assessment via surface motion monitoring using the ISBAS DInSAR technique over the Flow Country, Scotland. Remote. Sens. 10 (7), http://dx.doi.org/10.3390/rs10071103.

Ansari, H., De Zan, F., Bamler, R., 2018. Efficient Phase Estimation for Interferogram Stacks. IEEE Trans. Geosci. Remote Sens. 56 (7), http://dx.doi.org/10.1109/TGRS. 2018.2826045.

Arikan, M., Van Leijen, F., Guang, L., Hanssen, R., 2008. Improved image alignment under the influence of elevation. In: European Space Agency, (Special Publication)

Berardino, P., Fornaro, G., Lanari, R., Sansosti, E., 2002. A new algorithm for surface deformation monitoring based on small baseline differential SAR interferograms. IEEE Trans. Geosci. Remote Sens. 40 (11), http://dx.doi.org/10.1109/TGRS.2002. 803792

Berglund, Ö., Berglund, K., 2010. Distribution and cultivation intensity of agricultural peat and gyttja soils in Sweden and estimation of greenhouse gas emissions from cultivated peat soils. Geoderma 154 (3–4), http://dx.doi.org/10.1016/j.geoderma. 2008 11 035

Bhogapurapu, N., Siqueira, P., Armston, J., 2024. A New InSAR Temporal Decorrelation Model for Seasonal Vegetation Change With Dense Time-Series Data. IEEE Geosci. Remote. Sens. Lett. 21, 1–5. http://dx.doi.org/10.1109/LGRS.2024.3434653, URL: https://ieeexplore.ieee.org/document/10613793/.

Borger, G.J., 1992. Draining - digging - dredging; the creation of a new landscape in the peat areas of the low countries. http://dx.doi.org/10.1007/978-94-015-7997-1_4, Fens and bogs in the Netherlands.

Brouns, K., 2016. The effects of climate change on decomposition in Dutch peatlands: an exploration of peat origin and land use effects (Ph.D. thesis). Utrecht University, p. 190.

- Buckley, S.M., Rosen, P.A., Hensley, S., Tapley, B.D., 2003. Land subsidence in Houston, Texas, measured by radar interferometry and constrained by extensometers. J. Geophys. Res.: Solid Earth 108 (B11), http://dx.doi.org/10.1029/2002jb001848.
- Burbey, T.J., 2020. Extensometer forensics: what can the data really tell us? Hydrogeol. J. 28 (2), 637–655. http://dx.doi.org/10.1007/s10040-019-02060-6.
- Cain, M.R., Hensel, P.F., 2018. Wetland Elevations at Sub-Centimeter Precision: Exploring the Use of Digital Barcode Leveling for Elevation Monitoring. Estuaries Coasts 41 (2), 582–591. http://dx.doi.org/10.1007/s12237-017-0282-6, URL: http://link.springer.com/10.1007/s12237-017-0282-6.
- Conroy, P., 2025. Monitoring Highly Dynamic Land Surface Motion with Satellite Radar Interferometry (Ph.D. thesis). TU Delft, http://dx.doi.org/10.4233/uuid:491585b8-860a-4e5b-8e3e-97b4e23ae4ec.
- Conroy, P., van Diepen, S.A., Hanssen, R.F., 2023a. SPAMS: A new empirical model for soft soil surface displacement based on meteorological input data. Geoderma 440, 116699. http://dx.doi.org/10.1016/j.geoderma.2023.116699.
- Conroy, P., Lumban-Gaol, Y., Van Diepen, S., Van Leijen, F., Hanssen, R.F., 2024. First wide-area Dutch peatland subsidence estimates based on InSAR. In: IGARSS 2024-2024 IEEE International Geoscience and Remote Sensing Symposium. IEEE, pp. 10732–10735.
- Conroy, P., Van Diepen, S.A., Van Leijen, F.J., Hanssen, R.F., 2023b. Bridging Loss-of-Lock in InSAR Time Series of Distributed Scatterers. IEEE Trans. Geosci. Remote Sens. 61, http://dx.doi.org/10.1109/TGRS.2023.3329967.
- Corominas, J., Moya, J., Lloret, A., Gili, J.A., Angeli, M.G., Pasuto, A., Silvano, S., 2000. Measurement of landslide displacements using a wire extensometer. Eng. Geol. 55 (3), http://dx.doi.org/10.1016/S0013-7952(99)00086-1.
- Dawson, Q., Kechavarzi, C., Leeds-Harrison, P.B., Burton, R.G., 2010. Subsidence and degradation of agricultural peatlands in the Fenlands of Norfolk, UK. Geoderma 154 (3–4), http://dx.doi.org/10.1016/j.geoderma.2009.09.017.
- de Bakker, H., Schelling, J., 1989. Systeem van bodemclassificatie voor Nederland; De hogere niveaus (With English summary), second ed. Centrum voor Landbouwpublikaties en Landbouwdocumentatie, Wageningen, p. 218, URL: https://edepot.wur.nl/117844.
- de Vries, F., de Groot, W., Hoogland, T., Denneboom, J., 2003. De Bodemkaart van Nederland digitaal; Toelichting bij inhoud, actualiteit en methodiek en korte beschrijving van additionel informatie. Technical Report. Alterra Rapport 811, Wageningen: Alterra, Research Instituut voor de Groene Ruimte, Wageningen.
- Ferretti, A., Fumagalli, A., Novali, F., Prati, C., Rocca, F., Rucci, A., 2011. A new algorithm for processing interferometric data-stacks: SqueeSAR. In: IEEE Transactions on Geoscience and Remote Sensing. 49, (9), http://dx.doi.org/10.1109/TGRS.2011. 2124465.
- Fryksten, J., Nilfouroushan, F., 2019. Analysis of Clay-Induced Land Subsidence in Uppsala City Using Sentinel-1 SAR Data and Precise Leveling. Remote. Sens. 11 (23), 2764. http://dx.doi.org/10.3390/rs11232764, URL: https://www.mdpi.com/2072-4292/11/23/2764.
- Galloway, D.L., Burbey, T.J., 2011. Review: Regional land subsidence accompanying groundwater extraction. Hydrogeol. J. 19 (8), http://dx.doi.org/10.1007/s10040-011-0775-5.
- Hanssen, R.F., 2001. Radar Interferometry: Data Interpretation and Error Analysis (Remote Sensing and Digital Image Processing). Springer.
- Hoogland, T., van den Akker, J.J., Brus, D.J., 2012. Modeling the subsidence of peat soils in the Dutch coastal area. Geoderma 171–172, http://dx.doi.org/10.1016/j. geoderma.2011.02.013.
- Hooijer, A., Page, S., Jauhiainen, J., Lee, W.A., Lu, X.X., Idris, A., Anshari, G., 2011.

 Subsidence and carbon loss in drained tropical peatlands: reducing uncertainty and implications for CO 2 emission reduction options. Biogeosciences 8.
- Hu, F., Wu, J., Chang, L., Hanssen, R.F., 2019. Incorporating temporary coherent scatterers in multi-temporal insar using adaptive temporal subsets. IEEE Trans. Geosci. Remote Sens. 57 (10), 7658–7670. http://dx.doi.org/10.1109/TGRS.2019. 2915658
- Jiang, M., Ding, X., Hanssen, R.F., Malhotra, R., Chang, L., 2015. Fast statistically homogeneous pixel selection for covariance matrix estimation for multitemporal InSAR. IEEE Trans. Geosci. Remote Sens. 53 (3), http://dx.doi.org/10.1109/TGRS. 2014.2336237.
- Jiang, J., Lohman, R.B., 2021. Coherence-guided InSAR deformation analysis in the presence of ongoing land surface changes in the Imperial Valley, California. Remote Sens. Environ. 253, http://dx.doi.org/10.1016/j.rse.2020.112160.
- Kampes, B.M., Hanssen, R.F., Perski, Z., 2004. Radar interferometry with public domain tools. In: European Space Agency, (Special Publication) ESA SP. (550).
- Kampes, B., Usai, S., 1999. Doris: the Delft Object-oriented Radar Interferometric Software. In: 2nd International Symposium on Operationalization of Remote Sensing, vol. 1620.

- Liu, Y., Li, J., Fang, Z.N., 2019. Groundwater level change management on control of land subsidence supported by borehole extensometer compaction measurements in the houston-galveston region, Texas. Geosci. (Switzerland) 9 (5), http://dx.doi.org/ 10.3390/geosciences9050223.
- Liu, Y., Yang, H., Fan, J., Han, J., Lu, Z., 2022. NL-MMSE: A Hybrid Phase Optimization Method in Multimaster Interferogram Stack for DS-InSAR Applications. IEEE J. Sel. Top. Appl. Earth Obs. Remote. Sens. 15, http://dx.doi.org/10.1109/JSTARS.2022. 3208955.
- Lumban-Gaol, Y., Hanssen, R., 2025. SPAMS10 Delfland: Soil motion parameters to model relative surface elevation changes. http://dx.doi.org/10.4121/604b35a9-8e10-4044-8041-5effacaf6f8a.
- Maliva, R., Missimer, T., 2012. Compaction and Land Subsidence. In: Environmental Science and Engineering. http://dx.doi.org/10.1007/978-3-642-29104-3 15.
- Massop, H.T., Hessel, R., van den Akker, J.J., van Asselen, S., Erkens, G., Gerritsen, P.A., Gerritsen, F.H., 2024. Monitoring long-term peat subsidence with subsidence platens in Zegveld, The Netherlands. Geoderma 450, 117039. http://dx.doi.org/10.1016/j.geoderma.2024.117039, URL: https://linkinghub.elsevier.com/retrieve/pii/S0016706124002684.
- Miller, M.M., Jones, C.E., Sangha, S.S., Bekaert, D.P., 2020. Rapid drought-induced land subsidence and its impact on the California aqueduct. Remote Sens. Environ. 251, http://dx.doi.org/10.1016/j.rse.2020.112063.
- Morishita, Y., Hanssen, R.F., 2015. Deformation Parameter Estimation in Low Coherence Areas Using a Multisatellite InSAR Approach. IEEE Trans. Geosci. Remote Sens. 53 (8), http://dx.doi.org/10.1109/TGRS.2015.2394394.
- Parizzi, A., Brcic, R., 2011. Adaptive InSAR stack multilooking exploiting amplitude statistics: A comparison between different techniques and practical results. IEEE Geosci. Remote. Sens. Lett. 8 (3), http://dx.doi.org/10.1109/LGRS.2010.2083631.
- Pepe, A., Yang, Y., Manzo, M., Lanari, R., 2015. Improved EMCF-SBAS processing chain based on advanced techniques for the noise-filtering and selection of small baseline multi-look DInSAR interferograms. IEEE Trans. Geosci. Remote Sens. 53 (8), http://dx.doi.org/10.1109/TGRS.2015.2396875.
- Pierik, H.J., 2021. Landscape changes and human-landscape interaction during the first millennium AD in the Netherlands. Geol. En Mijnbouw/Netherlands J. Geosci. 100, http://dx.doi.org/10.1017/njg.2021.8.
- Querner, E., Jansen, P., Kwakernaak, C., 2008. Effects of water level strategies in Dutch peatlands: a scenario study for the polder Zegveld. Proc. the 13th Int. Peat Congr. International Peat Soc. Tullamore (January).
- Saari, T., Poutanen, M., Saaranen, V., Kaartinen, H., Kukko, A., Lahtinen, S., 2015. Height determination techniques for the next national height system of finland - a case study. Geod. Cartogr. 41 (4), 145–155. http://dx.doi.org/ 10.3846/20296991.2015.1120387, URL: https://journals.vilniustech.lt/index.php/ GAC/article/view/2847.
- Samiei-Esfahany, S., Martins, J.E., van Leijen, F., Hanssen, R.F., 2016. Phase Estimation for Distributed Scatterers in InSAR Stacks Using Integer Least Squares Estimation. IEEE Trans. Geosci. Remote Sens. 54 (10), 5671–5687. http://dx.doi.org/10.1109/ TGRS.2016.2566604, URL: http://ieeexplore.ieee.org/document/7501494/.
- Schothorst, C.J., 1977. Subsidence of low moor peat soils in the western Netherlands. Geoderma 17 (4), http://dx.doi.org/10.1016/0016-7061(77)90089-1.
- Schothorst, C.J., 1982. Drainage and behaviour of peat soils. In: International Institute for Land Reclamation and Improvement. ILRI Publication.
- Tampuu, T., Praks, J., Uiboupin, R., Kull, A., 2020. Long term interferometric temporal coherence and DInSAR phase in Northern Peatlands. Remote. Sens. 12 (10), http://dx.doi.org/10.3390/rs12101566.
- Ten Veen, J., Vis, G.-J., de Jager, J., Wong, T. (Eds.), 2025. Geology of the Netherlands, Second Edi Amsterdam University Press, Amsterdam, p. 914. http://dx.doi.org/10.5117/9789463728362, URL: https://library.oapen.org/handle/20.500.12657/100510.
- Teunissen, P., 2024. Testing Theory; an introduction, third ed. TU Delft OPEN Publishing, Delft, p. 151, URL: https://pure.tudelft.nl/ws/portalfiles/portal/214132690/Testing Theory.pdf.
- TU Delft, 2024. DECADE: DElft Contextually Aided Distributed scatterer Environment. URL: https://bitbucket.org/grsradartudelft/decade/src/main/.
- van Asselen, S., Erkens, G., De Graaf, F., 2020. Monitoring shallow subsidence in cultivated peatlands. Proc. Int. Assoc. Hydrological Sci. 382, 189–194. http://dx.doi.org/10.5194/piahs-382-189-2020.
- Van Den Akker, J., Jansen, P., Hendriks, R., Hoving, I., Pleijter, M., 2012. Submerged infiltration to halve subsidence and greenhouse gas emissions of agricultural peat soils. In: 14th International Peat Congress.
- Van Lanen, R.J., Kosian, M.C., 2020. What wetlands can teach us: reconstructing historical water-management systems and their present-day importance through GIScience. Water Hist. 12 (2), http://dx.doi.org/10.1007/s12685-020-00251-7.
- Vicente-Serrano, S.M., Beguería, S., López-Moreno, J.I., 2010. A Multiscalar Drought Index Sensitive to Global Warming: The Standardized Precipitation Evapotranspiration Index. J. Clim. 23 (7), 1696–1718. http://dx.doi.org/10.1175/2009JCLI2909.1, URL: http://journals.ametsoc.org/doi/10.1175/2009JCLI2909.1.